ARTICLES
https://doi.org/10.1038/s41567-020-0968-8

nature physics

Photo-excitation of long-lived transient intermediates in ultracold reactions

Yu Liu[1,2,3,6], Ming-Guang Hu[1,3,6], Matthew A. Nichols[1,3], David D. Grimes[1,3], Tijs Karman[4], Hua Guo[5] and Kang-Kuen Ni[1,2,3] ✉

In many chemical reactions, the transformation from reactants to products is mediated by transient intermediate complexes. For gas-phase reactions involving molecules with a few atoms, these complexes typically live on the order of 10 ps or less before dissociating, and are therefore rarely influenced by external processes. Here, we demonstrate that the transient intermediate complex K_2Rb_2*, formed from collisions between ultracold KRb molecules, undergoes rapid photo-excitation in the presence of a continuous-wave laser source at 1,064 nm, a wavelength commonly used to confine ultracold molecules. These excitations are facilitated by the exceptionally long lifetime of the complex under ultracold conditions. Indeed, by monitoring the change in the complex population after the sudden removal of the excitation light, we directly measure the lifetime of the complex to be 360 ± 30 ns, in agreement with our calculations based on the Rice–Ramsperger–Kassel–Marcus (RRKM) statistical theory. Our results shed light on the origin of the two-body loss widely observed in ultracold molecule experiments. Additionally, the long complex lifetime, coupled with the observed photo-excitation pathway, opens up the possibility to spectroscopically probe the structure of the complex with high resolution, thus elucidating the reaction dynamics.

Intermediate complexes have been studied extensively since the early days of chemistry[1–3] and continue to be an important subject of research today[4–7]. As the bridge between reactants and products, their structures, energetics and dynamics directly determine the rates and outcomes of chemical reactions. In gas-phase reactions, intermediate complexes are characterized by their fleeting nature—typically lasting on the order of 10 ps or less in systems consisting of a handful of atoms—and thus require ultrafast techniques to access their dynamics[8]. On the other hand, substantially longer-lived complexes have been predicted[9] and recently observed[10] in reactions between diatomic molecules that take place at ultralow temperatures. It was understood that the preparation of reactant molecules in their lowest rovibronic quantum states drastically reduced the number of exit channels available for complex dissociation, thus prolonging its lifetime. However, despite considerable progress in understanding the collisional properties of ultracold molecules over the past decade[11–13], direct information about the intermediate complexes, including their lifetimes, remains lacking.

The role of long-lived complexes has been discussed extensively in the context of ultracold collisions between rovibronic ground-state bialkali molecules (AB) where the atom-exchange pathway to reaction products ($AB + AB \rightarrow A_2 + B_2$) is energetically forbidden, but two-body loss of molecules was experimentally detected[14–17]. Such losses limit the phase-space densities achievable in these systems, and present a major obstacle to realizing novel quantum phases with long-range, dipolar interactions in bulk molecular samples[18–21]. It was proposed that a long-lived complex (A_2B_2*) allows time for a third body (a photon[22] or a molecule[9]) to interact with the complex, leading to the observed loss. However, the complex lifetimes calculated in these proposals differ widely[9,23], which stems from difficulties in estimating the density of states (DOS) of the complex and uncertainties in whether nuclei maintain their spins during reactions. The loss mechanisms therefore remain an open question.

In this Article, by studying reactive collisions between $^{40}K^{87}Rb$ molecules in the presence of varying intensities of 1,064-nm light, we observe rapid photo-excitation of the complex, manifested as a reduction in both the complex and the product populations. We determine the first-order rate constant for the excitation to be $0.42 \pm 0.09\,\mu s^{-1}\,(kW\,cm^{-2})^{-1}$, in agreement with our theoretical prediction. Exploiting this effect, we use light to induce complex loss and, after an abrupt shut-off of the light, monitor the time evolution of the complex population as it reaches a steady state to extract the complex lifetime. Our measurement agrees well with the calculated value based on Rice–Ramsperger–Kassel–Marcus (RRKM) theory[24] using full-dimensional ab initio potential energy surfaces (PESs).

Ultracold reactions in the presence of light

Each experiment begins with a gas of ~5,000 rovibronic ground-state KRb molecules prepared at a temperature of 500 nK and with an average number density of $3.5 \times 10^{11}\,cm^{-3}$ inside a crossed optical dipole trap (ODT) formed from two 1,064-nm laser beams ('H' and 'V'), as illustrated in Fig. 1a. Details of the apparatus regarding the production and detection of the gas have been reported previously[25]. As soon as the KRb sample is created inside the ODT, its density, n_r, decays via two-body loss, which can be characterized by $n_r(t) = n_r(t=0)(1 + t/t_{1/2})^{-1}$, where $t_{1/2}$ denotes the half-life, which is measured to be 250 ± 30 ms. In a previous study[10] it was determined that, in the absence of ODT light, this population decay occurs as a result of the exothermic bimolecular exchange reaction:

$$^{40}K^{87}Rb + {}^{40}K^{87}Rb \rightarrow K_2Rb_2^* \rightarrow K_2 + Rb_2 + 10\,cm^{-1} \quad (1)$$

[1]Department of Chemistry and Chemical Biology, Harvard University, Cambridge, MA, USA. [2]Department of Physics, Harvard University, Cambridge, MA, USA. [3]Harvard-MIT Center for Ultracold Atoms, Cambridge, MA, USA. [4]ITAMP, Harvard-Smithsonian Center for Astrophysics, Cambridge, MA, USA. [5]Department of Chemistry and Chemical Biology, University of New Mexico, Albuquerque, NM, USA. [6]These authors contributed equally: Yu Liu, Ming-Guang Hu. ✉e-mail: ni@chemistry.harvard.edu

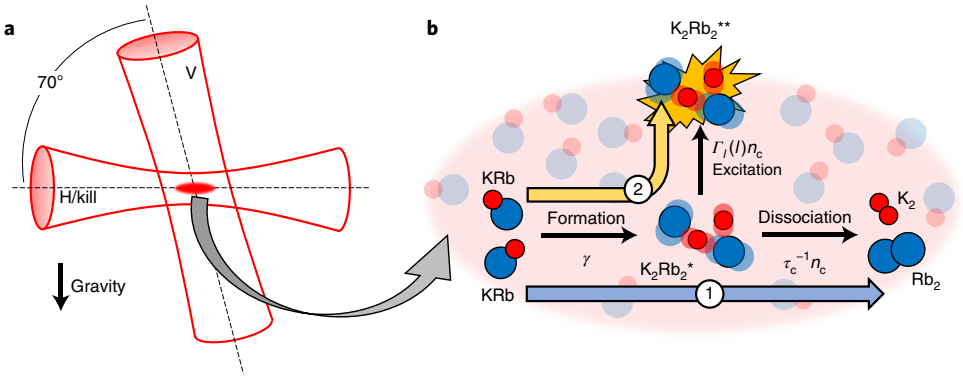

Fig. 1 | Ultracold reactions in an optical dipole trap. a, Optical trapping of a gas of KRb molecules. 'H' and 'V' are Gaussian beams with $1/e^2$ diameters of 60 and 200 μm, respectively. The 'kill' beam, introduced for the purpose of complex lifetime measurement, shares the same optical path with 'H', but has independent timing control. **b**, Two pathways for bimolecular KRb reactions. Both pathways involve the formation of a long-lived intermediate complex $K_2Rb_2^*$. '1' indicates the ground-state pathway $KRb + KRb \rightarrow K_2Rb_2^* \rightarrow K_2 + Rb_2$, which is the only pathway in the absence of ODT light; '2' indicates the excited-state pathway $KRb + KRb \rightarrow K_2Rb_2^* \rightarrow K_2Rb_2^{**}$, which is dominant at high ODT intensity. The rates for $K_2Rb_2^*$ formation, dissociation and excitation are labelled as γ, $\tau_c^{-1}n_c$ and $\Gamma_I(I)n_c$, respectively.

where * denotes the transient intermediate complex (Fig. 1b). In establishing this pathway, we concluded that the ODT did not contribute to the formation of the detected $K_2Rb_2^*$ complex. Here, we study this reaction in the presence of the ODT, and search for possible effects of the 1,064-nm light on the complex and products.

We first probe for changes in the amount of reaction products (K_2 and Rb_2) formed while the KRb cloud is exposed to varying intensities of ODT light. A simple change in the overall intensity of the ODT, however, would modify the confining potential felt by the KRb molecules and therefore the temperature and density of the gas, resulting in changes in the rate of reaction. To circumvent this issue, we apply a fast square-wave modulation to the ODT intensity (Fig. 2a, inset). This creates two phases with variable instantaneous intensity levels, I and I', while keeping the time-averaged intensity, $(I + I')/2$, constant. As long as the modulation frequency, f_{mod}, is much higher than the trapping frequencies of the gas, f_{trap}, the molecular motions are unaffected, and therefore the density, temperature and two-body loss rate of the gas remain unchanged. We fulfil this requirement by choosing $f_{mod} = 3\,\mathrm{kHz}$, where $f_{trap} \leq 0.4\,\mathrm{kHz}$ along all three axes of the trap.

As the reaction proceeds, we sample the product population using ion time-of-flight mass spectrometry (TOF-MS), the details of which have been described previously[10,25]. In brief, the region surrounding the KRb cloud is exposed to a pulsed ultraviolet ionization laser with a wavelength of 305 nm and a pulse duration of 7 ns. Photoionized products are then accelerated onto a time- and position-sensitive ion detector and counted. The total ion counts associated with each species serve as a proxy for its steady-state population at the instances of the ultraviolet pulses. The repetition of the ultraviolet pulses is synchronized to the ODT intensity modulation such that the reaction is always probed towards the end of the I phase, allowing the product distribution to settle into steady state after the previous I' phase.

We accumulated ion data at 10 different values of I between 0 and 22.6 kW cm^{-2}, with a fixed time-averaged intensity of 22.6 kW cm^{-2}. The counts of K_2^+ and Rb_2^+, plotted in Fig. 2a, decrease monotonically with increasing values of I, indicating a reduction in the amount of products formed as the ODT becomes more intense. We rule out electronic excitation of the products by the 1,064-nm light as the cause of this reduction, because the light is far-detuned from any relevant molecular transitions in K_2 (ref. [26]) and Rb_2 (ref. [27]). Additionally, we observe that the ion counts plateau at high ODT intensities to a value ~25% of the maximum signal, an effect that

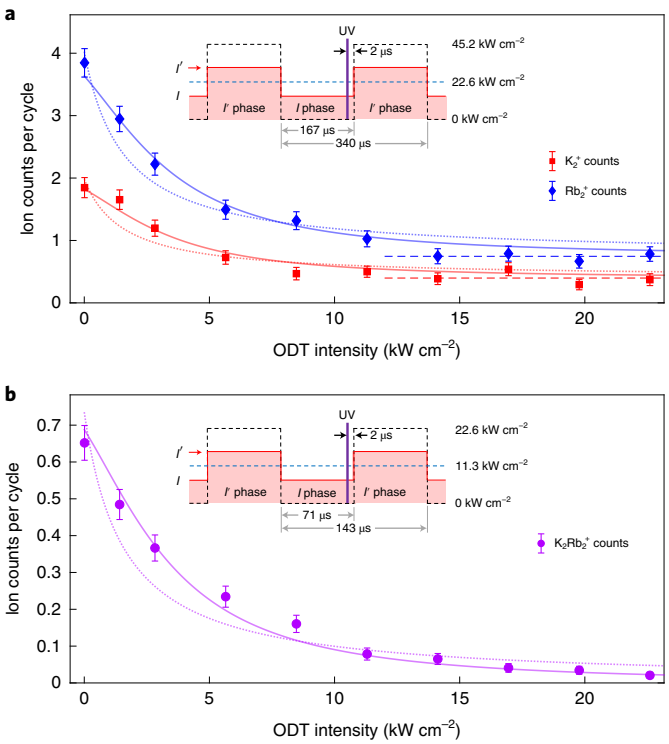

Fig. 2 | Trap light-induced excitation of the intermediate complex. a, Steady-state K_2^+ (red squares) and Rb_2^+ (blue diamonds) ion counts at various ODT light intensities, normalized by the number of experimental cycles (~80 for each data point). Error bars represent shot noise. The dashed lines indicate the offset levels $C_{K_2^+}$ and $C_{Rb_2^+}$. **b**, Steady-state $K_2Rb_2^+$ (purple circles) ion counts at various ODT light intensities, normalized by the number of experimental cycles (~290 for each data point). Solid lines are simultaneous fits to the data in **a** and **b** using equation (5), with B_1 and B_2 as free parameters, and the dotted lines are fits with B_2 set to zero and only B_1 as a free parameter. The fits are weighted by the inverse of the ion counts. Insets: timing schemes for the ODT (red) and the pulsed UV ionization laser (purple) used for the product and complex measurements. The blue dashed line represents the time-averaged intensity level and the black dashed line represents the ODT intensity envelope for full depth modulation.

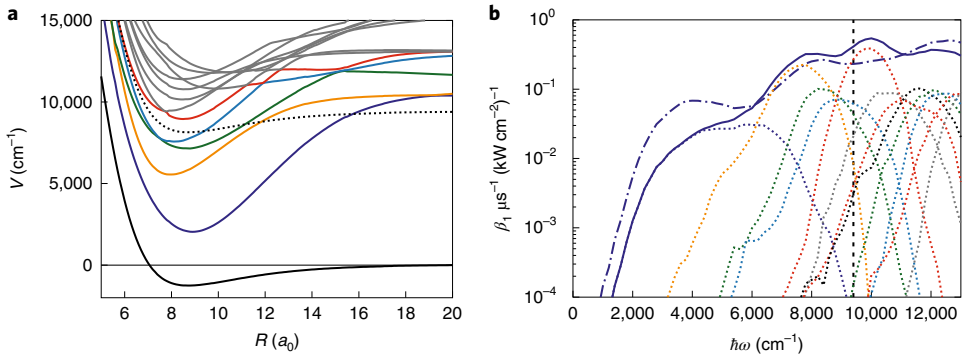

Fig. 3 | Energies and rates of the electronic excitations of the complex. a, Potential energy curves for the ground state and low-lying excited states of KRb + KRb as a function of the distance between the molecules, R, in units of the Bohr radius, a_0, for fixed orientation and monomer bond lengths. The black dotted curve shows the ground-state potential shifted vertically by the energy of a 1,064-nm photon. This crosses various excited-state potentials, indicating these are accessible through one-photon excitation of the complex. **b**, Calculated excitation rates as a function of the excitation photon energy, with the 1,064-nm ODT marked by the vertical dashed line. Dotted lines show the contribution of various adiabatic electronic states, colour-coded in agreement with the potential curves in **a**. The blue solid line shows the corresponding total excitation rate, whereas the dashed-dotted line shows the excitation rate obtained assuming the total dipole moment is equally distributed over all excited states. The difference between the two serves as an indication of the uncertainty in the calculated transition dipole moments.

persists up to at least 45.2 kW cm^{-2}, as we have independently verified (see Methods).

Because products are formed from the dissociation of the K_2Rb_2* complexes, it is natural to question how the complexes are affected by the ODT light. To this end, we probe the complex population at different ODT intensities using an experimental protocol similar to that used for the products (Fig. 2b, inset). Here, the ultraviolet ionization laser is tuned to 354.77 nm, a wavelength that results in the photo-ionization of K_2Rb_2* into $K_2Rb_2^+$ (ref. [10]). The intensity of the ODT is then modulated at $f_{mod} = 7$ kHz with a time-averaged value of 11.3 kW cm^{-2}. $K_2Rb_2^+$ ion counts were accumulated at 10 different values of I between 0 and 22.6 kW cm^{-2}, as shown in Fig. 2b.

Similar to the products, the complex population also decreases with increasing intensity of the 1,064-nm light. This observation points to photo-induced complex loss, as postulated in ref. [22]. To verify this hypothesis, we computed the energies and rates of electronic excitations of K_2Rb_2 using an ab initio method. The results show that multiple excited states can be reached by the absorption of a single 1,064-nm photon, with an appreciable transition rate at most of the ODT intensities explored here (Fig. 3). This indicates that, in addition to the previously observed ground-state pathway, there is a competing excited-state pathway (Fig. 1b):

$$\mathrm{KRb} + \mathrm{KRb} \rightarrow \mathrm{K_2Rb_2}^{*} \xrightarrow{h\nu} \mathrm{K_2Rb_2}^{**} \tag{2}$$

The photo-excited complex, K_2Rb_2**, is the likely source of the offset observed at high ODT intensities in the product data of Fig. 2a. Possible channels for the formation of K_2 and Rb_2 from K_2Rb_2** include dissociation via crossings with repulsive potentials, and decay via spontaneous emission into product-forming channels on the ground-state PES. Products resulting from these processes will, in general, have different translational energy distributions from those formed via the ground-state reaction pathway, which provides an avenue for future investigations into their origins.

We include both pathways to model the data in Fig. 2 using the rate equation

$$\dot{n}_c(t) = \gamma - \tau_c^{-1} n_c(t) - \Gamma_l(I) n_c(t) \tag{3}$$

where n_c is the complex density, $\gamma = -\dot{n}_r/2$ is the rate of KRb + KRb collisions, τ_c is the complex lifetime and Γ_l is the intensity-dependent photo-excitation rate. In the steady state, formation of the complex from reactants is balanced by its dissociation into products and its photo-excitation, so that $\dot{n}_c = 0$. In this case, the complex density is given by

$$n_c = \frac{\gamma}{\tau_c^{-1} + \Gamma_l(I)} \tag{4}$$

We model the excitation rate as $\Gamma_l = \beta_1 I + \beta_2 I^2$, where the linear term represents single-photon excitation of the complex, and the quadratic term represents possible second-order contributions. Equation (4) then becomes $n_c = \gamma\tau_c(1 + B_1 I + B_2 I^2)^{-1}$, where $B_{1,2} = \beta_{1,2}\tau_c$. Because both the product and the complex ion counts are proportional to the steady-state density of the complex, their dependence on the 1,064-nm light intensity can be modelled as

$$N_s = \frac{A_s}{1 + B_1 I + B_2 I^2} + C_s \tag{5}$$

where $s = K_2^+$, Rb_2^+ or $K_2Rb_2^+$, and C_s is introduced to account for any offsets in the data. We apply equation (5) to simultaneously fit the product and complex ion data, as shown in Fig. 2a,b. For the product data, C_s is fixed to be the average value of the respective set of four data points at the highest ODT intensities, while for the complex data, C_s is set to zero. We allow the amplitudes A_s to be independent free parameters, whereas B_1 and B_2 are shared parameters across the datasets. The fit adequately captures the data in all three sets, and yields $B_1 = 0.15 \pm 0.03$ cm^2 kW^{-1} and $B_2 = 0.050 \pm 0.004$ (cm^2 kW^{-1})^2, with a mean-squared-error (m.s.e.) of 1.2. Alternatively, we fit the three datasets in Fig. 2 with B_2 set to zero, representing an excitation rate model that is purely linear in the intensity. In this case we find that $B_1 = 0.64 \pm 0.05$ cm^2 kW^{-1}, but that the fit yields a larger m.s.e. of 4.0 and systematically underestimates the lower intensity data points while overestimating the higher ones. This indicates that the linear rate model is insufficient to fully describe the observed photo-excitation of the complex.

We note that the term $B_1 I + B_2 I^2$ physically represents the ratio between the rates of complex excitation and dissociation. Given the values for $B_{1,2}$ obtained from the fit with the smaller m.s.e., we find that, at a typical ODT intensity of 11.3 kW cm^{-2}, the

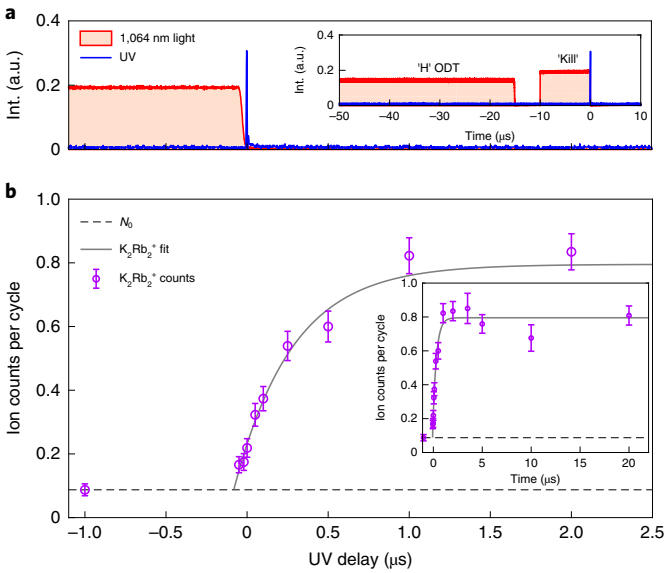

Fig. 4 | Lifetime of the intermediate complex. a, Measured time traces of the 1,064-nm light (red) and the ultraviolet ionization pulse (blue) intensities. The ultraviolet pulses probe the complex population around the off edge of the 'kill' pulse, which provides a zero-of-time for the measurements. Inset: the same traces displayed over a wider time window showing the relative timing between the 'H' and 'kill' beams. The 'V' beam, not shown here, shares the same timing as the 'H' beam. With the addition of the 'kill' beam, the 'H' beam power is adjusted such that the time-averaged intensity of the ODT is maintained at 11.3 kW cm^{-2}. **b**, $K_2Rb_2^+$ ion counts (purple circles) measured at different ultraviolet delays with respect to the off edge of the 'kill' pulse. The dashed line indicates the baseline from which the ion counts grow after the light is turned off. The level for this baseline is given by the ion counts at −1 μs, N_0. Error bars represent shot noise. The solid line shows a fit to the entire dataset (see inset) using the function $A\left(1-(1-N_0/A)\mathrm{e}^{-(t-t_0)/\tau_c}\right)$, which is derived from equation (6). The fit yields a complex lifetime $\tau_c = 360 \pm 30$ ns, and a timing offset $t_0 = -82 \pm 7$ ns. This offset accounts for a systematic uncertainty in the relative timing between the 1,064-nm light and the ultraviolet. The m.s.e. for the fit is 0.85.

reaction is approximately eight times as likely to proceed via the excited-state pathway as the ground-state pathway. In contrast, if the complex lifetime were to be of order 10 ps or less, as is typically found in higher-temperature reactions, the effects of the photo-excitation would become negligible at any reasonably achievable optical power.

Measuring the complex lifetime

The lifetime of the intermediate complex has been measured for a variety of chemical systems[28–30], where the use of ultrafast lasers and molecular beam techniques establishes a well-defined zero-of-time for all individual reaction events, allowing the process of complex formation and dissociation to be monitored in real time. In our experiment, the bulk nature of the ultracold KRb sample makes establishing a zero-of-time challenging, as individual reactions occur stochastically. Fortunately, the observed optical excitation of the complex makes it possible to use light to set a zero-of-time. Specifically, we first strongly reduce the complex population by exposing the KRb cloud to intense 1,064-nm light, and then monitor its growth to a new steady-state value after the light is quickly switched off. In this situation, the kinetics of the complex density can be understood by solving equation (3) with the initial condition $n_c(t=0) = n_0$, where $t=0$ is the time at which the light turns off, and n_0 is the suppressed complex density at and before the turn-off. The solution is given by

$$n_c(t) = \gamma\tau_c\left(1-\left(1-\frac{n_0}{\gamma\tau_c}\right)\mathrm{e}^{-t/\tau_c}\right) \quad (6)$$

where the 1/e saturation time is the complex lifetime τ_c. Note that equation (6) is exact if the light turns off instantaneously, and is a good approximation if the characteristic turn-off time $t_{off} \ll \tau_c$. To minimize t_{off}, we introduce a 'kill' beam whose wavelength and optical path are identical to the 'H' beam (Fig. 1a), but whose timing and intensity are independently controlled. This 'kill' beam has a 90–10% fall time of 30 ns, compared to >200 ns for the 'H' and 'V' beams.

As the reaction proceeds, the intensities of the ODT beams are modulated with 100% depth at 7 kHz. During the dark phase of the modulation, the 'kill' beam is pulsed on for 10 μs with an intensity of 12.7 kW cm^{-2}, and the ultraviolet pulse probes the complex population at various delay times around the off edge of the 'kill' pulse (Fig. 4a). Here, we define $t=0$ as the time when the ultraviolet pulse is delayed 27 ns with respect to the midpoint of the 'kill' pulse turn-off. The $K_2Rb_2^+$ counts are plotted against the ultraviolet delay in Fig. 4b and fitted using the function $N_{K_2Rb_2^+} = A\left(1-(1-N_0/A)\mathrm{e}^{-(t-t_0)/\tau_c}\right)$, derived from equation (6), with A, t_0 and τ_c as free parameters. Here, t_0 is introduced to account for a systematic timing uncertainty, and N_0 is fixed to the ion counts measured at an ultraviolet delay of −1 μs, when the 'kill' pulse is still on, which serves as a proxy for n_0. The complex lifetime given by the fit is 360 ± 30 ns.

Having measured both τ_c and $B_{1,2} = \beta_{1,2}\tau_c$, we can determine the first- and second-order rate constants, β_1 and β_2, for complex excitation by 1,064-nm light. For $B_1 = 0.15 \pm 0.03$ cm^2 kW^{-1} and $B_2 = 0.050 \pm 0.004$ (cm^2 kW^{-1})^2 extracted from the fit to the data in Fig. 2, we obtain $\beta_1 = 0.42 \pm 0.09$ μs^{-1} (kW cm^{-2})$^{-1}$ and $\beta_2 = 0.14 \pm 0.02$ μs^{-1} (kW cm^{-2})$^{-2}$.

Theory and comparison

Finally, we perform theoretical calculations of both the lifetime and the photo-excitation rate of the complex and compare them to the measurements. We assume that the complex explores the reaction phase space ergodically before dissociating into products/reactants and estimate the lifetime using RRKM theory[24], $\tau_c = 2\pi\hbar\rho_c/\mathcal{N}$. Here, ρ_c is the DOS of the complex and $\mathcal{N}$ is the number of open product channels via which the complex can dissociate. We also assume that, over the course of the reaction, the total angular momentum of the system ($J=1$) is conserved (see Methods) and the spins of the nuclei remain unchanged. $\mathcal{N}$ is counted using known values for the exothermicity of the reaction[31] and the rotational constants of K_2 (ref. [32]) and Rb_2 (ref. [33]). Computing ρ_c requires knowledge of the ground-state PES for the KRb + KRb system, which we calculate in full dimensionality using the Molpro package[34] (see Methods). A one-dimensional cut of the PES is shown in Fig. 3a. Using this PES and following the quasi-classical method developed in ref. [23], we calculate ρ_c to be 2.6 ± 0.8 μK^{-1}. The uncertainty is estimated by scaling the potential by ±15%. The resulting RRKM lifetime is 170 ± 60 ns, which is remarkably similar to the measured value. Although we have assumed that nuclear spins do not change during the reaction, the calculated lifetime is expected to be comparable even if they do, because any additional hyperfine channels will increase both ρ_c and $\mathcal{N}$ by similar proportions, whereas the RRKM lifetime depends only on the ratio of the two.

To calculate the first-order photo-excitation rate constant, we compute excitation energies and transition dipole moments for the lowest 12 excited states. The single-photon excitation rate of the complex from the ground state, i, to a particular excited state, f, is computed as $\Gamma_{i\to f} = c^{-1}\langle b_{i\to f}(\omega)\rangle I$. Here, c is the speed of light, I is the

optical intensity, ω is the excitation frequency and b is the Einstein B-coefficient for state f. Under the assumption that the complex ergodically explores the ground PES, b can be calculated by averaging the squared transition dipole moment over the local DOS[22]. Contributions from different excited states are then summed to obtain the total excitation rate Γ_l. The rate constant, $\beta_1 = \Gamma_l/I$, is shown in Fig. 3b as a function of the excitation photon energy. At 1,064 nm, this excitation rate is $\beta_1 = 0.4^{+0.4}_{-0.2}\,\mu s^{-1}\,(kW\,cm^{-2})^{-1}$, which agrees well with the measured first-order excitation rate of $0.42 \pm 0.09\,\mu s^{-1}\,(kW\,cm^{-2})^{-1}$. Calculation of the second-order rate constant, β_2, requires an understanding of higher-order excitation processes in the complex, which is beyond the scope of the current work.

Conclusions and outlook

Our identification of the photo-excited reactive pathway in an ultracold KRb gas not only brings new understanding to the origin of molecular loss in this much-studied system[10,31,35], but also has important implications for the losses observed in other ultracold bialkali species whose ground-state reactive pathways are energetically forbidden[14–17]. Because the electronic structures of these systems are comparable to KRb, the complexes formed from bimolecular collisions are also susceptible to excitations and losses induced by the trapping light, as suggested by ref. [22]. Avoiding this pathway may therefore facilitate the creation of molecular gases with higher phase-space densities and the exploration of the many new scientific directions such systems promise[19,21,24,36]. From the perspective of controlling chemical reactions, the long-lived complex formed from ultracold molecular collisions provides a new handle to steer the reaction dynamics. Studying the decay pathways for the optically excited complex may allow for direct control of reaction outcomes using light. By further combining quantum-state readout of the reaction complexes and products, ultracold molecules offer the opportunity to investigate bond breaking and formation at the microscopic level.

Note added in proof: During the preparation of this manuscript, we became aware of a related parallel experimental work[37].

Online content

Any methods, additional references, Nature Research reporting summaries, source data, extended data, supplementary information, acknowledgements, peer review information; details of author contributions and competing interests; and statements of data and code availability are available at https://doi.org/10.1038/s41567-020-0968-8.

Received: 28 February 2020; Accepted: 16 June 2020;
Published online: 20 July 2020

References

1. Light, J. C. Statistical theory of bimolecular exchange reactions. *Discuss. Faraday Soc.* **44**, 14–29 (1967).
2. Herschbach, D. Reactive scattering. *Faraday Discuss. Chem. Soc.* **55**, 233–251 (1973).
3. Troe, J. The Polanyi Lecture. The colourful world of complex-forming bimolecular reactions. *J. Chem. Soc. Faraday Trans.* **90**, 2303–2317 (1994).
4. Su, Y.-T., Huang, Y.-H., Witek, H. A. & Lee, Y.-P. Infrared absorption spectrum of the simplest Criegee intermediate CH_2OO. *Science* **340**, 174–176 (2013).
5. Bjork, B. J. et al. Direct frequency comb measurement of OD + CO → DOCO kinetics. *Science* **354**, 444–448 (2016).
6. Continetti, R. E. & Guo, H. Dynamics of transient species via anion photodetachment. *Chem. Soc. Rev.* **46**, 7650–7667 (2017).
7. Osborn, D. L. Reaction mechanisms on multiwell potential energy surfaces in combustion (and atmospheric) chemistry. *Annu. Rev. Phys. Chem.* **68**, 233–260 (2017).
8. Zewail, A. H. Femtochemistry: atomic-scale dynamics of the chemical bond. *J. Phys. Chem. A* **104**, 5660–5694 (2000).
9. Mayle, M., Quéméner, G., Ruzic, B. P. & Bohn, J. L. Scattering of ultracold molecules in the highly resonant regime. *Phys. Rev. A* **87**, 012709 (2013).
10. Hu, M.-G. et al. Direct observation of bimolecular reactions of ultracold KRb molecules. *Science* **366**, 1111–1115 (2019).
11. Quemener, G. & Julienne, P. S. Ultracold molecules under control! *Chem. Rev.* **112**, 4949–5011 (2012).
12. Balakrishnan, N. Perspective: ultracold molecules and the dawn of cold controlled chemistry. *J. Chem. Phys.* **145**, 150901 (2016).
13. Lique, F. et al. *Cold Chemistry: Molecular Scattering and Reactivity Near Absolute Zero* (Royal Society of Chemistry, 2017).
14. Takekoshi, T. et al. Ultracold dense samples of dipolar RbCs molecules in the rovibrational and hyperfine ground state. *Phys. Rev. Lett.* **113**, 205301 (2014).
15. Ye, X., Guo, M., González-Martínez, M. L., Quéméner, G. & Wang, D. Collisions of ultracold $^{23}Na^{87}Rb$ molecules with controlled chemical reactivities. *Sci. Adv.* **4**, eaaq0083 (2018).
16. Gregory, P. D. et al. Sticky collisions of ultracold RbCs molecules. *Nat. Commun.* **10**, 3104 (2019).
17. Park, J. W., Will, S. A. & Zwierlein, M. W. Ultracold dipolar gas of fermionic $^{23}Na^{40}K$ molecules in their absolute ground state. *Phys. Rev. Lett.* **114**, 205302 (2015).
18. Santos, L., Shlyapnikov, G., Zoller, P. & Lewenstein, M. Bose–Einstein condensation in trapped dipolar gases. *Phys. Rev. Lett.* **85**, 1791–1794 (2000).
19. Büchler, H. P. et al. Strongly correlated 2D quantum phases with cold polar molecules: controlling the shape of the interaction potential. *Phys. Rev. Lett.* **98**, 060404 (2007).
20. Levinsen, J., Cooper, N. R. & Shlyapnikov, G. V. Topological $p_x + ip_y$ superfluid phase of fermionic polar molecules. *Phys. Rev. A* **84**, 013603 (2011).
21. Baranov, M. A., Dalmonte, M., Pupillo, G. & Zoller, P. Condensed matter theory of dipolar quantum gases. *Chem. Rev.* **112**, 5012–5061 (2012).
22. Christianen, A., Zwierlein, M. W., Groenenboom, G. C. & Karman, T. Photoinduced two-body loss of ultracold molecules. *Phys. Rev. Lett.* **123**, 123402 (2019).
23. Christianen, A., Karman, T. & Groenenboom, G. C. Quasiclassical method for calculating the density of states of ultracold collision complexes. *Phys. Rev. A* **100**, 032708 (2019).
24. Levine, R. D. *Molecular Reaction Dynamics* (Cambridge Univ. Press, 2009).
25. Liu, Y., Grimes, D. D., Hu, M.-G. & Ni, K.-K. Probing ultracold chemistry using ion spectrometry. *Phys. Chem. Chem. Phys.* **22**, 4861–4874 (2020).
26. Vadla, C. et al. Comparison of theoretical and experimental red and near infrared absorption spectra in overheated potassium vapour. *Eur. Phys. J. D* **37**, 37–49 (2006).
27. Edvardsson, D., Lunell, S. & Marian, C. M. Calculation of potential energy curves for Rb_2 including relativistic effects. *Mol. Phys.* **101**, 2381–2389 (2003).
28. Sato, H. Photodissociation of simple molecules in the gas phase. *Chem. Rev.* **101**, 2687–2726 (2001).
29. Noll, R. J., Yi, S. S. & Weisshaar, J. C. Bimolecular $Ni^+(^2D_{5/2}) + C_3H_8$ reaction dynamics in real time. *J. Phys. Chem. A* **102**, 386–394 (1998).
30. Scherer, N., Sipes, C., Bernstein, R. & Zewail, A. Real-time clocking of bimolecular reactions: application to $H + CO_2$. *J. Chem. Phys.* **92**, 5239–5259 (1990).
31. Ospelkaus, S. et al. Quantum-state controlled chemical reactions of ultracold potassium-rubidium molecules. *Science* **327**, 853–857 (2010).
32. Huber, K.-P. *Molecular Spectra and Molecular Structure: IV. Constants of Diatomic Molecules* (Springer, 2013).
33. Amiot, C. Laser-induced fluorescence of Rb_2: the $(1)^1\Sigma_g^+(X)$, $(2)^1\Sigma_g^+(X)$, $(1)^1\Pi_u(B)$, $(1)^1\Pi_g$, and $(2)^1\Pi_g(C)$ electronic states. *J. Chem. Phys.* **93**, 8591–8604 (1990).
34. Werner, H.-J. et al. Molpro, version 2019.2, a package of ab initio programs (Molpro, 2019); http://www.molpro.net
35. De Marco, L. et al. A degenerate Fermi gas of polar molecules. *Science* **363**, 853–856 (2019).
36. Yao, N. Y., Zaletel, M. P., Stamper-Kurn, D. M. & Vishwanath, A. A quantum dipolar spin liquid. *Nat. Phys.* **14**, 405–410 (2018).
37. Gregory, P. D., Blackmore, J. A., Bromley, S. L. & Cornish, S. L. Loss of ultracold ^{87}Rb ^{133}Cs molecules via optical excitation of long-lived two-body collision complexes. *Phys. Rev. Lett.* **124**, 163402 (2020).

Methods

Experimental set-up. The ODT for the KRb molecules is formed by the crossing of two Gaussian beams, 'H' and 'V', with $1/e^2$ waist diameters of 60 and 200 μm, respectively, at a 70° angle (Fig. 1a). At a total optical intensity of 11.3 kW cm^{-2}, this trap configuration results in a cigar-shaped cloud of KRb molecules with 2σ Gaussian widths of 6, 6 and 28 μm along its three principal axes. Thus, the ODT intensity varies by less than 4% over these widths and is considered to be constant across the sample. All ODT beams are derived from a single 1,064-nm laser source with a spectral width of 1 kHz.

Weak static electric (17 V cm^{-1}) and magnetic (5 G) fields are applied during the experiment, for the purposes of extracting ions for TOF-MS and maintaining nuclear spin quantization for the KRb molecules, respectively. The direction of the electric field is normal to the plane containing the ODT beams, whereas the magnetic field is anti-parallel to the gravity direction.

Quantum states of the reactants and the products. The reactant KRb molecules are prepared in the $|m_I^{\mathrm{K}} = -4, m_I^{\mathrm{Rb}} = 1/2\rangle$ hyperfine state of the lowest rovibronic state, $|X^1\Sigma^+, v = 0, N = 0\rangle$, where m_I, v and N are the nuclear spin projection, molecular vibration and molecular rotation quantum numbers, respectively. The product K_2 and Rb_2 molecules emerge from reactions in their respective vibrational ground states, but with rotational excitations of up to $N_{\mathrm{K_2}} = 13$ and $N_{\mathrm{Rb_2}} = 21$.

Photo-ionization of the products and the complex. As the reaction proceeds, the products, K_2 and Rb_2, escape from the ODT due to translational energy gained from the exothermicity, and establish steady-state density distributions, $n_{\mathrm{K_2}}$ and $n_{\mathrm{Rb_2}}$, around the KRb cloud. Because products are generated at the same rate at which the K_2Rb_2* complex dissociates, $n_{\mathrm{K_2}}$ and $n_{\mathrm{Rb_2}}$ are both proportional to the complex density n_c. The photon energy at the wavelength used to ionize products (305 nm) is above the ionization threshold of KRb. To selectively ionize the products, and not the reactants inside the ODT, the pulsed ultraviolet laser is shaped into a ring-shaped beam profile centred around the KRb cloud, with a diameter of 0.45 mm and a 1σ Gaussian width of 5.4 μm. The complexes, on the other hand, reside within the ODT due to their negligible lab-frame translational energy and their transient nature. To photo-ionize them, the ultraviolet laser is shaped into a Gaussian beam with a $1/e^2$ waist diameter of 300 μm that overlaps the KRb cloud. Fortunately, the photon energy at the wavelength used here (354.77 nm) is below the ionization threshold of KRb and does not result in measurable depletion of the KRb molecules.

Ion counts as proxies for product and complex densities. Although the data presented in Fig. 2 are in the form of ion counts, $N_{\mathrm{K_2}^+}$, $N_{\mathrm{Rb_2}^+}$ and $N_{\mathrm{K_2Rb_2}^+}$, the modelling of these data is based on the instantaneous density of the K_2Rb_2* complex, n_c. Here, we establish the proportionality between the detected ion counts and the complex density, starting with a derivation of the relationship between $N_{\mathrm{K_2Rb_2}^+}$ (equation (5)) and n_c (equation (4)). The pre-factor $\gamma = -\dot{n}_r/2$ in equation (4) describes the decay of the complex density within each experimental cycle arising from the decay of the KRb population, which has a half-life of hundreds of milliseconds. Consider a single ionization ultraviolet pulse that probes the system at a time t after the creation of the KRb sample. Because the pulse is a few nanoseconds in duration, it maps the complex density at that time onto a detected ion count

$$N^{\mathrm{single}}_{\mathrm{K_2Rb_2}^+}(t) = P_{\mathrm{ion}}\eta_{\mathrm{det}}V_{\mathrm{trap}}\gamma(t)\frac{1}{\tau_c^{-1}+\Gamma_l} \tag{7}$$

where P_{ion} is the ionization probability, η_{det} is the ion detection efficiency and V_{trap} is the effective volume of the trap. In each experimental cycle, a newly prepared KRb sample is probed by a total of 7,000 ultraviolet pulses over a duration of 1 s. The total ion count per cycle is therefore

$$N_{\mathrm{K_2Rb_2}^+} = \left[P_{\mathrm{ion}}\eta_{\mathrm{det}}V_{\mathrm{trap}}\sum_{m=1}^{7{,}000}\gamma(mT)\right]\frac{1}{\tau_c^{-1}+\Gamma_l} \tag{8}$$

where $T = 143$ μs is the period of the ultraviolet pulses. Note that the bracketed pre-factor is a constant, which we call A in equation (5). This shows that $N_{\mathrm{K_2Rb_2}^+}$ is indeed proportional to n_c. Following analogous arguments, it can be shown that the product ion counts, $N_{\mathrm{K_2}^+}$ and $N_{\mathrm{Rb_2}^+}$, are also proportional to the associated densities, $n_{\mathrm{K_2}}$ and $n_{\mathrm{Rb_2}}$, which are in turn proportional to n_c. The same logic applies with regard to the relationship between the time-dependent ion counts and the complex density for the complex lifetime measurement shown in Fig. 4.

Reaching a steady state following a change in the instantaneous ODT intensity. When the ODT intensity is switched from the I' phase to the I phase (Fig. 2, insets), the density of the complex evolves into a new steady-state value on a timescale equal to or less than the complex lifetime τ_c, which we have measured to be 360 ± 30 ns. The products, on the other hand, take longer a time to re-establish their steady-state density distribution around the KRb cloud, due to the finite speed with which they escape the ODT. This timescale, which depends on the diameter of the hollow UV beam (0.45 mm) and the typical speed of the products (a few to a few tens of metres per second), is empirically determined to be ~100 μs. Thus, for both the product and the complex measurements shown in Fig. 2, there is a sufficient separation in time between the intensity switch and the ultraviolet pulse such that we probe the steady-state complex and product densities during the I phase.

Continued formation of products at high ODT intensities. We measure the dependence of the product ion counts on the ODT intensity in the 11.3–46.2 kW cm^{-2} range, which partially overlaps with, but extends beyond the range probed in Fig. 2a. For these measurements, the intensity of the ODT is modulated with full contrast, but with a variable duty cycle $D = t_{\mathrm{on}}/T$, where the ODT is on for a duration of t_{on} within each cycle of period T, which is chosen to be 500 μs. The time-averaged ODT intensity, I_{avg}, is kept constant at 11.3 kW cm^{-2}. For a given duty cycle D, the intensity I during the on-phase is $I = I_{\mathrm{avg}}/D$. The ultraviolet ionization pulses then probe the products shortly (2 μs) after the ODT is turned off. As this time is much shorter than the time it takes to perturb the product density distribution at the location of the ionization ring (~100 μs), the detected product density accurately reflects that during the on-phase of the ODT. The normalized product ion counts at different ODT intensities are shown in Extended Data Fig. 1. The inset shows the timing diagram for the intensities of the ODT and the pulsed ultraviolet ionization laser. We observe a plateau in the ion counts for $I \geq 15$ kW cm^{-2}, indicating continued product formation despite the high ODT intensity. This plateau justifies our choice of using the average value of the high intensity data points in Fig. 2a to provide a baseline for the fitting.

Theory methods. To calculate the ground-state PES for the KRb + KRb system, we use polarizable effective core potentials[38] and solve the electronic Schrödinger equation for the four valence electrons using the multi-reference configuration interaction in a large one-electron basis set[39]. Ab initio points are computed for ~2,000 geometries, selected using Latin hypercube sampling, and fitted using Gaussian Process regression[39]. The minimum energy structures agree with those of ref. [40] as well as ref. [41], and the corresponding binding energies in these three independent calculations differ by less than 15%, which we take to be the uncertainty of the energy calculation.

In computing the DOS of the intermediate complex, ρ_c, we counted only states that satisfy the conservation of total angular momentum **J** throughout the reaction[23]. On the reactant side, **J** consists of the orbital angular momentum of the relative motion between the colliding KRb molecules, **L**, as well as the rotations of the molecules about their internal axes, $\mathbf{N}_{\mathrm{KRb(1)}}$ and $\mathbf{N}_{\mathrm{KRb(2)}}$, that is, $\mathbf{J} = \mathbf{L} + \mathbf{N}_{\mathrm{KRb(1)}} + \mathbf{N}_{\mathrm{KRb(2)}}$. Because reactant KRb molecules, prepared in a single hyperfine quantum state, are identical fermions, their collisions at ultralow temperatures are restricted to the lowest partial wave with odd parity, the p-wave, where $L = 1$. Additionally, because the KRb molecules are in the rotational ground state, their rotational quantum number is $N = 0$. As a result, the total angular momentum for the KRb + KRb system is $J = 1$.

Excitation energies and transition dipole moments are calculated at the complete active space self-consistent field level, using methods otherwise similar to the ground-state calculation. The uncertainty in the calculated excitation rate is limited by the poor fit of the transition dipole surfaces, caused by crossings of adiabatic excited states at which the transition dipole functions are not analytic. Therefore, we also perform calculations where we fit the total squared transition dipole moment, which is unaffected by crossings between excited states, and distribute this squared dipole moment equally over all excited states. The resulting excitation rate is smaller by a factor of two (Fig. 3b), which we take to be indicative of the uncertainty due to the dipole surfaces.

Data availability

The data that support the findings of this study are available from the corresponding author upon reasonable request. Source data are provided with this paper.

Code availability

The computer codes used for theoretical calculations in this study are available from T.K. (tijs.karman@cfa.harvard.edu) upon reasonable request.

References

38. Fuentealba, P., Preuss, H., Stoll, H. & Von Szentpály, L. A proper account of core-polarization with pseudopotentials: single valence-electron alkali compounds. *Chem. Phys. Lett.* **89**, 418–422 (1982).
39. Christianen, A., Karman, T., Vargas-Hernández, R. A., Groenenboom, G. C. & Krems, R. V. Six-dimensional potential energy surface for NaK–NaK collisions: Gaussian process representation with correct asymptotic form. *J. Chem. Phys.* **150**, 064106 (2019).
40. Byrd, J. N., Montgomery, J. A. Jr & Côté, R. Structure and thermochemistry of K_2Rb, KRb_2, and K_2Rb_2. *Phys. Rev. A* **82**, 010502 (2010).
41. Yang, D. et al. A global full-dimensional potential energy surface for the K_2Rb_2 complex and its lifetime. *J. Phys. Chem. Lett.* **11**, 2605–2610 (2020).

Acknowledgements

We thank L. Zhu for experimental assistance. This work is supported by DOE YIP and the David and Lucile Packard Foundation. M.A.N. is supported by an HQI postdoctoral fellowship. T.K. is supported by NWO Rubicon grant no. 019.172EN.007 and the NSF through ITAMP. H.G. acknowledges a MURI grant from ARO (W911NF-19-1-0283) and a Humboldt Research Award.

Author contributions

The experimental work and data analysis were carried out by Y.L., M.-G.H., M.A.N., D.D.G. and K.-K.N. Theoretical calculations were performed by T.K., and H.G. aided in the analysis of the results. All authors contributed to interpreting the results and writing the manuscript.

Competing interests

The authors declare no competing interests.

Additional information

Extended data is available for this paper at https://doi.org/10.1038/s41567-020-0968-8.

Supplementary information is available for this paper at https://doi.org/10.1038/s41567-020-0968-8.

Correspondence and requests for materials should be addressed to K.-K.N.

Reprints and permissions information is available at www.nature.com/reprints.

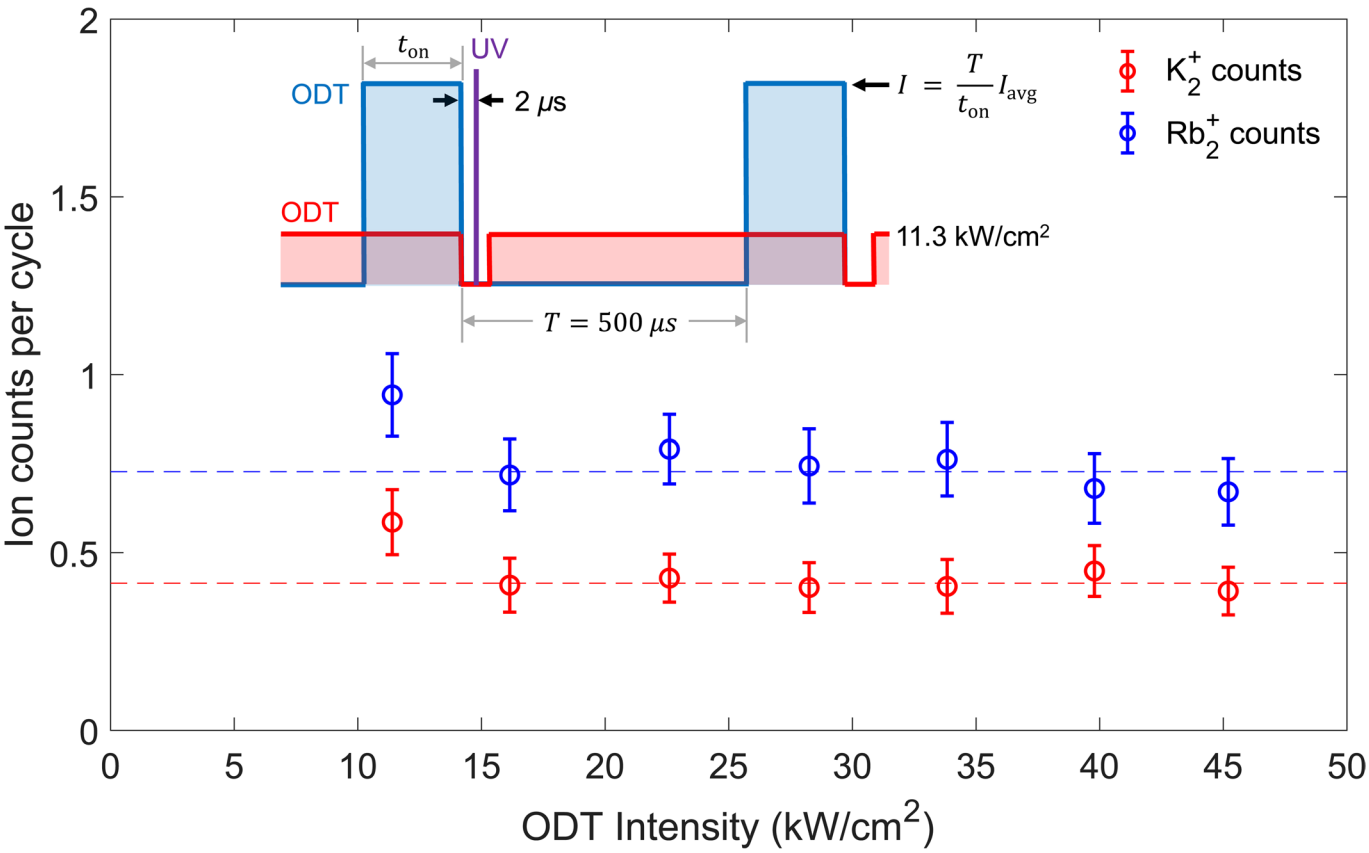

Extended Data Fig. 1 | Continued formation of products at high ODT intensities. Steady-state K_2^+ (red circles) and Rb_2^+ (blue circles) ion counts at ODT light intensities in the 11.3–46.2 kW/cm^2 range, normalized by the number of experimental cycles (~ 80 for each data point). The error bars represent shot noise. The dashed lines indicate the levels to which the ion counts plateau, obtained by averaging, within each dataset, the values of the points at ODT intensities larger than 15 kW/cm^2. (Inset) Timing schemes of the ODT (red and blue) and the pulsed UV ionization laser (purple) used for the measurements presented here. The red (blue) trace corresponds to a high (low) duty cycle modulation of the ODT. The instantaneous ODT intensity, I, is inversely proportional to the duty cycle, while the time-averaged ODT intensity, I_{avg} is constant for all measurements.